Extracellular enzyme activity in the coastal upwelling system off Peru: a mesocosm experiment

Kristian Spilling[1,2,*], Jonna Piiparinen[1], Eric P. Achterberg[3], Javier Arístegui[4], Lennart T. Bach[5], Maria T. Camarena-Gómez[1], Elisabeth von der Esch[6], Martin A. Fischer[7], Markel Gómez-Letona[4], Nauzet Hernández-Hernández[4], Judith Meyer[3], Ruth A. Schmitz[7], Ulf Riebesell[3]

1. Marine Research Centre, Finnish Environment Institute, Helsinki, Finland

2. Centre for Coastal Research, University of Agder, Kristiansand Norway

3. GEOMAR Helmholtz Centre for Ocean Research Kiel, Kiel, Germany

4. Instituto de Oceanografía y Cambio Global, IOCAG, Universidad de Las Palmas de Gran Canaria, Las Palmas de Gran Canaria, Spain

5. Institute for Marine and Antarctic Studies, University of Tasmania, Tasmania, Australia

6. Institute of Hydrochemistry, Chair of Analytical Chemistry and Water Chemistry, Technical University of Munich, Munich, Germany

7. Institute for General Microbiology, Christian Albrechts University Kiel, Germany

*corresponding author: kristian.spilling@syke.fi

Abstract

The Peruvian upwelling system is a highly productive ecosystem with a large oxygen minimum zone (OMZ) close to the surface. Here, we carried out a mesocosm experiment off Callao, Peru, with the addition of water masses from the regional OMZ collected at two different sites simulating two different upwelling scenarios. Here we focus on pelagic remineralization of organic matter by extracellular enzyme activity of leucine aminopeptidase (LAP) and alkaline phosphatase activity (APA). After addition of the OMZ water, dissolved inorganic nitrogen (N) was depleted, but the standing stock of phytoplankton was relatively high even after nutrient depletion (mostly >4 µg chlorophyll *a* L^{-1}). During the initial phase of the experiment, APA was 0.6 nmol L^{-1} h^{-1} even though the PO_4^{3-} concentration was >0.5 µmol L^{-1}. Initially, the dissolved organic phosphorus (DOP) decreased, coinciding with an increase in PO_4^{3-} concentration probably linked to the APA. The LAP activity was very high with most of the measurements in the range 200-800 nmol L^{-1} h^{-1}. This enzyme hydrolyzes terminal amino acids from larger molecules (e.g. peptides or proteins), and these high values are probably linked to the highly productive, but N-limited coastal ecosystem. Also, the experiment took place during a rare coastal El Niño event with higher-than-normal surface temperatures, which could have affected enzyme activity. Using a non-parametric multidimensional scaling analysis (NMDS) with a generalized additive model (GAM), we found that biogeochemical variables (e.g. nutrient and chlorophyll *a* concentrations), phytoplankton and bacterial communities explained up to 64% of the variability in APA. The bacterial community explained best the variability (34%) in LAP. The high hydrolysis rates for this enzyme suggests that pelagic N remineralization, likely driven by the bacterial community, supported the high standing stock of primary producers in the mesocosms after N depletion.

Introduction

The Peruvian upwelling system is one of the most productive marine ecosystems in the world (FAO, 2018). Its high productivity is driven by the upwelling of deep, nutrient rich water that fuels primary production when reaching the sunlit surface. The primary limiting nutrient is nitrogen (N), but iron (Fe) availability is also an important driver for phytoplankton biomass production in addition to light (Chavez et al., 2008; Messié and Chavez, 2015). Part of the phytoplankton biomass passes to higher trophic levels through grazing and predation. As the upwelled water parcel is transported further offshore by Ekman transport, part of the biomass settles out of the euphotic zone and is decomposed in intermediate water layers creating an extensive oxygen minimum zone (OMZ; Kalvelage et al., 2013). The fate of the biomass produced is consequently of great importance for higher trophic levels and for biogeochemical cycles

After inorganic nutrients (primarily N) have been depleted, primary production in the surface layer is driven by recycled production. In this process, dissolved organic matter (DOM) must first be broken down into simpler forms before the DOM elements become biologically available. The decomposition of DOM is not a uniform process as it is affected by both abiotic and biotic variables. Extracellular enzymes hydrolyze complex dissolved organic molecules and is the first step in remineralization of these DOM elements (Arnosti, 2011). Quantifying the rates of pelagic remineralization is important for understanding recycled production and element fluxes in the uppermost water masses. There are a range of different enzymes that are used for

hydrolyzing DOM, and two of the most studied ones are Leucine aminopeptidase (LAP) and Alkaline phosphatase (AP).

LAP hydrolyzes terminal amino acids from larger molecules (e.g. peptides or proteins) and is used extracellularly in aquatic systems by bacteria, some phytoplankton and fungi (Hoppe et al., 1988; Stoecker and Gustafson, 2003; Gutiérrez et al., 2011). It hydrolyses a broad spectrum of substrates with a free amino group, but it has preference for N-terminal leucine and related amino acids in peptides and proteins (Burley et al., 1990; Steen et al. 2015).

The AP enzyme is produced by a wide range of different organisms including aquatic bacteria and phytoplankton. Its main function is related to the hydrolysis of phosphate monoesters that separate orthophosphate (PO_4) from an organic compound (Perry, 1972; Hoppe, 2003). AP exists either as ectoenzyme (on the cell wall) or is excreted extracellularly, and for phytoplankton it has commonly been related to P-limitation in aquatic environments (Rose and Axler, 1997; Nausch, 1998). Bacterial AP activity (APA) is more complex, as some, especially particle attached bacteria, take up and use C and N from the organic molecule after hydrolysis, and may for this reason produce AP even under P replete conditions (Benitez-Nelson and Buesseler, 1999; Hoppe, 2003; Labry et al., 2016).

The ongoing warming of surface waters caused by climate change is projected to have several consequences on marine ecosystems. For example, increasing temperatures lead to a reduction in gas solubility causing a decrease in oxygen concentrations; warming will also increase thermal stratification and reduce the ventilation of the deeper ocean (Keeling et al., 2010). Both of these effects will lead to expanding OMZs with potential consequences for biogeochemical cycling (Oschlies et al., 2018). Biogeochemical cycles of nitrogen (N) and phosphorus (P) are affected

by O_2 depletions, e.g., through denitrification and sediment P release (Canfield et al., 2005). Hence, expanding OMZs may decrease the inorganic N : P ratio in the upwelled water potentially affecting the seston (i.e. all suspended particles) stoichiometry and plankton community composition (Hauss et al., 2012; Spilling et al., 2019).

In this study, a mesocosm experiment off the coast of Peru was carried out to study the effect of OMZ water to the surface, with several papers covering different aspects in this special issue. Here we were interested in the dynamics of organic matter break down. We measured the extracellular LAP and AP activities and used a statistical model to relate it to biogeochemical variables, and plankton and bacterioplankton communities. Our main aim was to understand how much of the variability in enzyme activities could be explained by biogeochemical variables (e.g. nutrient concentrations) and microbial communities.

Materials and methods

A detailed description of the mesocosm set up and collection and addition of OMZ-water can be found in Bach et al. (2020) within this special issue. Some of the basic variables such as inorganic nutrient concentration can also be found in Bach et al (2020). In short, the mesocosm bags were 2 m in diameter and extended from the surface down to 19 m depth, where the last 2 m was a conical sediment trap. Eight mesocosm bags were used and they were moored at 12.0555°S; 77.2348°W just north of Isla San Lorenzo where the water depth is ~30 m. The mesocosms were closed by attaching the sediment trap to the bottom and pulling the top above the surface on 25 Feb, 2017. The bags were regularly cleaned from the inside and outside. For a full detailed sampling and cleaning timetable see Bach et al. (2020).

Water (100 m^3) from the oxygen minimum zone (OMZ) was collected from two locations and depths. The first was collected from 12.028323°S; 77.223603°W from 30 m depth, and the second one from 12.044333°S; 77.377583°W from 70 m depth. The original aim was to collect severe and moderate OMZ signature water (differing in e.g. nitrate concentrations) from the first and second site, respectively. This assumption was based on long-term monitoring data, however, the chemical properties (e.g. nitrate concentration) was more similar in these water masses than anticipated, rather reflecting low and very low OMZ signatures from site 1 and 2 respectively. This was discovered only after the collection, and it was not technically possible to make additional collections of OMZ water. For this reason the data presented here focus on the temporal trend more than the difference between the two treatments, but for easier comparisons with the other papers in this special issue we keep the same graphical interface.

To have a baseline of measured variables, the mesocosms where closed and environmental and biological variables were determined over 10 days. After this period, the OMZ water was added to the mesocosms in two steps on day 11 and 12 after the enclosure of the mesocosms. As the mesocosms contain a specific volume (~54 m^3), the process of adding the OMZ water started with first removing water from the mesocosms. The water removed (~20 m^3) was pumped out from 11-12 m depth. A similar volume of OMZ water, from both collection sites, was then pumped into four replicate mesocosms each. The OMZ water was pumped into the mesocosms moving the input hose between 14-17 m depth. The water collected at 30 m depth was pumped into mesocosms M1, M4, M5 and M8 having a low OMZ signature and water from 70 m depth into mesocosms M2, M3, M6 and M7 having a very low OMZ signature. Due to the halocline at 12 m depth (see below), the added OMZ water was not immediately mixed throughout the mesocosm bag.

At the site of the mesocosms, the OMZ is normally close to the surface (<10 m depth; Graco et al., 2017) and consequently the bottom part of the mesocosm was low in oxygen. To keep the stratification inside the mesocosm we added 69 L of concentrated brine on day 13 by carefully inserting it between 12.5-17 m depth. The same procedure was repeated on day 33 when 33 L of brine was added. This artificial halocline prevented complete mixing of the mesocosm and the lower part of the mesocosm had a very different water chemistry compared to the upper 10 m were we did all our sampling. Right after the experiment, a third addition of brine was carried out to measure the total volume of the mesocosms.

Sampling took place every second day over a period of 50 days, and all variables were taken with an integrated water sampler (HydroBios, IWS) pre-programed to fill from 0 – 10 m depth and all samples consisted of this integrated samples from the upper 10 m. The samples were stored dark in cool boxes and brought back to the laboratory and processed right away. Sampling took place in the morning, and the samples were usually back in the laboratory around noon.

Nutrient concentrations

Inorganic nutrients were determined from filtered (0.45 µm filter, Sterivex, Merck) samples immediately after the water arrived in the laboratory. For the measurements, we used a continuous flow analyzer (QuAAtro AutoAnalyzer, SEAL Analytical) connected to a fluorescence detector (FP-2020, JASCO). Phosphate (PO_4^{3-}), nitrate (NO_3^-) and nitrite (NO_2^-) were determined colorimetrically (Murphy and Riley, 1962; Morris and Riley, 1963) and corrected with the refractive index method reported by Coverly et al. (2012). Ammonium (NH_4^+) concentrations were determined fluorometrically (Kérouel and Aminot, 1997). Dissolved

inorganic nitrogen (DIN) was calculated by summing NO_3^-, NO_2^- and NH_4^+. Further details on measurement accuracy can be found in Bach et al. (2020), where the individual DIN elements are also presented.

To measure total dissolved nitrogen (TDN) and phosphorus (TDP), the samples were first filtered through pre-combusted (5 h, 450°C) Whatman GF/F filters (pore size 0.7 µm). The filtrate was collected in 50 mL acid-cleaned high-density polyethylene (HDPE) bottles and placed directly into a freezer (-20°C). Later the filtrates were thawed at room temperature over a period of 24 hours and divided in two parts. The first half was used to determine inorganic nutrient concentrations as described above. From the other half we determined the TDN and TDP concentrations. An oxidizing reagent (Oxisolv, Merck) was added, and the samples were autoclaved for 30 minutes. TDN and TDP were measured spectrophotometrically (QuAAtro, Seal Analytical). Dissolved organic nitrogen (DON) concentrations were calculated by subtracting DIN from TDN. Dissolved organic phosphorus (DOP) was calculated as the difference between TDP and PO_4^{3-}.

Fluorescent dissolved organic matter and PARAFAC analysis

Fluorescent dissolved organic matter (FDOM) was determined by measuring fluorescence in water samples with a Cary Eclipse (Agilent Technologies) spectrofluorometer, using excitation and emission slit widths of 10 nm. Wavelength ranges were set to 230-456 nm for excitation, with 2 nm increments, and the 290-600 nm for emission with 5 nm increments. The measurements were collected into excitation-emission matrices (EEM). Blanks were measured with the same settings using ultrapure water.

Raw measurements were processed using the DOMFluor toolbox (v. 1.7; Stedmon and Bro, 2008) for Matlab (R2017a). The processing consisted of 1) blank subtraction from seawater EEMs, 2) EEMs normalization to the Raman area (RA), estimated applying the trapezoidal rule of integration on the emission scan at the 350 nm excitation wavelength in the blank EEMs, and 3) cropping of the 1st and 2nd order Rayleigh scatter bands. Inner filter correction was not performed as for the duration of the experiment the absorption coefficient at 250 nm (a_{250}) displayed values (mean ± sd = 1.56 ± 0.91 m^{-1}) well below 10 m^{-1}, above which correction is considered necessary (Stedmon and Bro, 2008).

The processed EEMs were analyzed applying a Parallel Factor Analysis (PARAFAC) using the DOMFluor toolbox. The PARAFAC model was constructed based on 125 samples (outliers were removed) and validated using split-half validation and random initialization. The resulting model consisted of 4 components (C1-C4; supplementary material Fig S1). For each of them, the fluorescence maximum (Fmax) was recorded. The identified fluorophores were compared to others found in the literature using the OpenFluor database (openfluor.lablicate.com; Murphy et al., 2014).

Phytoplankton community and chlorophyll a

Flow Cytometry subsamples were transferred from the IWS into 50 mL beakers and stored cool in the dark until analysis max. 8 hours after sampling. Each sample (650 µL) was analyzed with an Accuri C6 flow cytometer (BD Biosciences) set to a high flow rate (i.e. 66 µL/min).

Phytoplankton groups were differentiated based on the strength of the forward scatter (FSC-A), the side scatter (SSC-A), the red fluorescence (FL3-A) and orange fluorescence (FL2-A) signal ("A" refers to the area of the signal integral). Furthermore, we used sequential filtrations with different polycarbonate filters (Whatman, pore-sizes 0.2, 0.4, 0.8, 2, 3, 5, 8 µm) to distinguish populations in the cytogram based on size. This procedure was helpful to approximate how FSC-A values corresponded with size. We defined the following phytoplankton groups: Synechococcus-like cells (Syn; 0.2-2µm), Cryptophyte-like cells (Crypto; ~90% between 2-5 µm), picoeukaryotes (Peuks; 0.2-2 µm), Nanoeukaryotes (Nano; 2-20 µm, mostly in the lower range), Microeukaryotes 1 (Mikro1; ~15-40 µm, occasionally overlapping with Nano), Microeukaryotes 2 (Mikro2; ~>40 µm, cluster dominated by *Akashiwo sanguineum* from about day 20 onward), elongated cells "chains" determined by the ratio of FSC-A to FSC-H where "H" refers to the height of the forward scatter signal (details about this approach are provided in Paul et al., this issue. The goal of this was to detect chain-forming diatoms which we expected to be an important component of the community).

Samples for chlorophyll *a* (chl-*a*) determination were filtered onto GF/F filters (Whatman) and flash frozen in liquid nitrogen and stored at -80 °C (or dry ice for a brief period during air transfer; ~2 days) until measurement. The chl-*a* was extracted in acetone and the concentration was measured using high-performance liquid chromatography calibrated against commercial standards (Barlow et al., 1997). The chl-*a* autofluorescence of the phytoplankton community was measured with a handheld fluorometer (AquaPen, Photon Systems Instruments) using 450 nm excitation light. The photochemical efficiency was calculated based on the relationship between the variable to maximal fluorescence (Fv/Fm).

16S-rRNA gene based bacterial community determination

One liter of surface water obtained from the individual sampling sites was filtered through sterile Millipore Express PLUS membrane filters (polyethersulfon) with a cut-off of 0.22 µm and a diameter of 47 mm (Merck Millipore). After filtration, the filters were flash frozen in liquid nitrogen and stored at -80°C until nucleic acid extraction. Nucleic acid extraction was performed using the NucleoSpin TriPrep- Kit (Machery-Nagle) according to manufacturer's instruction with an additional step at the beginning of the extraction using a pestle to homogenize the sample.

Primers applied for the amplification of the bacterial 16S rRNA gene fragments were annealing to the variable region 1 and 2 and consisted of an initial standardized Illumina adapter (regular), followed by an 8 nucleotide barcode (X's), a linker region (underlined) and a primer sequence (bold). The sequences were for the forward primer Bac27 5'-AATGATACGGCGACCACCGAGATCTACACXXXXXXXXTATGGTAATTGT**AGAGTTTGATCCTGGCTCAG**-3' and reverse Bac338 5'-CAAGCAGAAGACGGCATACGAGATXXXXXXXXAGTCAGTCAGCC**TGCTGCCTCCCGTAGGAGT**-3'. The individual PCR reaction contained 100 ng of the extracted DNA. PCR conditions and purification of the amplification product were previously described (Fischer et al. 2019a). The final library pool for sequencing was combined from the eluates and contained 100 ng of DNA. Amplicon library sequencing was performed on a MiSeq instrument. Library therefore was prepared according to the manufacturer's instructions and sequenced using the v3 chemistry with 2 x 300bp paired-end.

Reads generated with amplicon sequencing were trimmed using the trimmomatic software version 0.33 (Bolger et al., 2014) as described in Fischer et al. (2019b). Briefly, reads were analyzed with a sliding window of 4 bp and regions were trimmed if the average Phred score (Ewing and Green, 1998; Ewing et al., 1998) within the window was below 30. Trimmed reads were kept within the dataset if the forward and reverse read both survived the quality trimming and were longer than 36 bp. Afterwards, 20,000 reads per sample were kept in the dataset (exceptions were sample M1 on day 10 (5817 reads) and M7 on day 24 (17660 reads) for further analysis.

Quality trimmed sequences were analyzed using MOTHUR software, version 1.35.1 (Schloss et al., 2009) as described in Fischer et al. (2019a). The quality filtered and subsampled reads were concatenated to 1,040,321 contiguous sequences (contigs) using the command make.contig. Contigs were filtered for ambiguous bases, homopolymers longer than 8 bases or sequences longer than 552 bases using the command screen.seqs. The resulting 754,310 contigs were checked for redundant sequences using the command unique.seqs and clustered to 199,746 unique sequences. The sequences were consecutively aligned to a modified version of the SILVA database release version 132 (Pruesse et al., 2012) containing only the hypervariable regions V1 and V2 by the command align.seqs. Sequences not aligning in the expected region were removed from the dataset using the command screen.seqs. The alignment was further optimized by removing gap-only columns with the command filter.seqs. The alignment contained 717,217 sequences (148,760 unique). Rare and closely related sequences were clustered using the commands unique.seqs and precluster.seqs. The latter was used to cluster sequences with up to 3 positional differences compared to larger sequence clusters together. Chimeric sequences were removed using the implemented software UCHIME (Edgar et al.,

2011) using the command chimera.uchime, followed by remove.seqs leaving 551,142 sequences (29,519 unique) in the dataset. The classification of the sequences was performed against the SILVA database and was done with a bootstrap threshold of 80 %. Operational taxonomic units (OTUs) were formed using the average neighbor clustering method with the command cluster.split. A sample-by-OUT table on the 97 % level, containing 10,258 OTUs, was generated using the command make.shared. These OTUs were used for the subsequent analysis. After the removal of mitochondria, chloroplast and singletons, 3225 OTUs were retained. These OTUs were used for downstream analysis.

Extracellular enzymes

The leucine aminopeptidase (LAP) activity was determined using the method described by Stoecker and Gustafson (2003) using *L*-leucine 7-amido-4-methyl-coumarin (Leu-AMC; Sigma Aldrich) as a substrate. Leu-AMC was added to a final concentration of 500 µmol L^{-1}, which was determined in separate kinetics tests to saturate the enzyme activity. The samples (100-200 µl) were incubated in the dark at in situ surface temperature for four to six hours. The fluorescence was measured every 30-60 min with a Cary Eclipse (Agilent Technologies) spectrofluorometer using 380 nm excitation and 440 nm emission wavelengths. The results were compared with a standard curve determined using 7-amino-4-methyl-coumarin (AMC; Sigma Aldrich) dissolved in DMSO, and the LAP activity calculated by linear regression.

Measurements of alkaline phosphatase activity (APA) were conducted with 20 ml subsamples of initial/incubated seawater using 100 nmol L^{-1} 4-methylumbelliferyl phosphate (MUF-P; Sigma-Aldrich) as the organic phosphate substrate (Ammerman, 1993). From this incubation, samples

were transferred into a well plate and fluorescence was measured on a BIOTEK Microplate Reader with a Cary Eclipse (Agilent Technologies) spectrofluorometer using 355 nm excitation light and 460 nm emission detection. Following MUF-P addition, fluorescence measurements were performed at 0, 1.5, and 3 h and APA (h^{-1}) was calculated from the linear increase in fluorescence and calibrated against 4-methylumbelliferone (MUF; Sigma-Aldrich). The assays were performed and incubated in the dark. Ultrapure water (Milli-Q) blanks and paraformaldehyde-killed controls generally yielded fluorescence values similar to $t = 0$ readings.

Statistical analysis

Before comparisons of enzyme activity between the two experimental treatments (OMZ water added from two different locations) were conducted, we first constructed a cumulative value where each measured value was summed up for each sampling day. The linear regressions of the cumulative enzyme activity from the two treatments (n = 4) were compared with Student's t-test. In addition, the effect of biogeochemical, phytoplankton and bacterioplankton community composition to APA and LAP was determined, using the ordination scores of the first and second axis of a non-parametric multidimensional scaling (NMDS) as explanatory variables in generalized additive models (GAMs) with APA or LAP as dependent variable. The NMDS was applied separately to each group of variables: biogeochemical, phytoplankton community and bacterioplankton community. The individual explanatory power of each MDS score was estimated with a univariate GAM. The visualization of the links was done for each explanatory variable through the prediction from the full model object, setting all other explanatory variables

at their mean value. In addition, links to the scores of the biogeochemical variables and phytoplankton community NMDS were estimated with one GAM model. It was not possible to include the bacterioplankton community into this model due to the different sampling regime (lower number of samples) and this was treated with a second model. NMDS was estimated with the metaMDS function in the Vegan package (Oksanen et al., 2017), and GAMs were fitted using the gam function in the mgcv package (Wood, 2017). For explaining the deviance, an adjusted coefficient of determination (R^2) was used. An adjusted R^2 takes into account the model complexity and is more conservative than a non-adjusted R^2.

RESULTS

Nutrients

Inorganic nutrients, dissolved inorganic nitrogen (DIN) and phosphate, were available for the two first weeks of the experiment (Fig 1). The addition of OMZ-water increased the phosphate concentrations whereas the dissolved inorganic nitrogen (DIN) was >2 µmol L^{-1} in the mesocosms until the addition of OMZ-water (days 11 and 12 of the experiment). After the addition of the OMZ-water, the DIN concentration rapidly declined and was depleted at day 15 in most mesocosms except in M3 where DIN depletion occurred a week later (day 22; Fig 1). The PO_4^{3-} concentration increased after closing the mesocosm and reached ~1.9 µmol L^{-1} in all mesocosms after the OMZ-water addition. There was only a slight reduction to approximately 1.5 µmol PO_4^{3-} L^{-1} over the course of the experiment (Fig 1).

The dissolved organic nitrogen (DON) and phosphorus (DOP) concentrations were initially 9 – 12 µmol L^{-1} and 0.6 – 1.0 µmol L^{-1}, respectively. There was no drastic change in DON with the OMZ-water addition and there was an overall decrease in DON to 6.0 - 7.9 µmol L^{-1} on day 30 after which it increased somewhat again. The DOP concentrations decreased rapidly the first 8 days to 0.19 - 0.32 µmol L^{-1} but increased after the OMZ-water addition and remained within 0.2 - 0.7 µmol L^{-1} interval for the rest of the experiment.

The PARAFAC modelling of the EEMs yielded four FDOM components (C1-C4; Fig 2 and S1). Using the OpenFluor database we identified multiple fluorophores with strong similarity ($TCC_{ex \cdot em} > 0.95$) to our components (Table S1). Components 1 and 3 had characteristics resembling amino acid/protein-like fluorescence, whereas the fluorescence of components 2 and 4 was humic-like (Table S1). All FDOM components increased sharply at day 18. This did not take place in Pacific seawater sampled outside the mesocosm where the FDOM was relatively stable throughout the experiment. After the increase at day 18, humic-like components (C2 and C4) were relatively stable but decreased slightly after day 28-30. The amino acid-like components (C1 and C3) exhibited higher variability among mesocosms, and C3 had overall higher variability throughout the experiment. Both humic-like and amino acid-like components maintained fluorescence values above the initial ones until the end of the experiment, but there were no clear differences between the treatments. However, towards the end of the experiment M1 and M2 had highest fluorescence values of C1. M1 also had highest values of C2 and C3 whereas M3 had the highest values of C4 at the end of the experiment.

Chlorophyll, photochemical efficiency and phytoplankton community

After OMZ-water addition, the chl-*a* concentration increased from 2-4 µg L^{-1} to 4-8 µg L^{-1} except for mesocosms M3 and M4 where the increase was not as pronounced (Fig 3). The chl-*a* concentration in M3 increased after day 22 to ~4 µg Chl-*a* L^{-1}, whereas in M4 the chl-*a* concentration remained low (<2 µg L^{-1}) throughout most of the experiment (Fig 3). The photochemical efficiency (Fv/Fm) was approximately 0.7 throughout the whole experiment without major difference between mesocosms, except for M4 where it was consistently lower (<0.6) during the last week of experiment (Fig 3).

The initial community was dominated by diatoms in terms of biomass but this group gradually reduced in numbers after the enclosure of the mesocosms and instead the mixotrophic dinoflagellate *Akashiwo sanguineum* appeared (Fig 4). The cell counts done with the flow cytometer were checked with a microscope and this was the primary species in terms of biomass in the Microeukaryote 2 group (Fig 4). The exceptions were mesocosms M3 and M4 where this dinoflagellate was not abundant (M4) or bloomed later (M3) and where there were more Chrysophytes. In M4 there was in addition a bloom of picoeukaryotes starting after day 20 (Fig 4). The parallels of the same treatment did not develop in the same way in all the mesocosms, and this was particularly evident from the phytoplankton community composition (Fig 4).

Bacterial community

The bacterial community was dominated by the class Alphaproteobacteria throughout the whole experiment and in all the mesocosms units, reaching values between 60 to 88% of the total sequences at day16 (Fig 5). Within Alphaproteobacteria, the *Roseobacter* lineage (genera HIMB11, *Ascidiaceihabitans*, *Amylibacter* and *Planktomarina* in M1) of the order

Rhodobacterales contributed most to the bacterial community in all the mesocosms (10-55 %) in particular on day 16, except in M8 where the SAR11 Ia clade dominated the community (55% of the total sequence at day 16). The order Parvibaculales had high relative abundances (12-20% of the total sequences) in M4, M5, M6 and M7 before the OMZ-water addition (day 10) decreasing in the following week. The relative abundance of order Rickettsiales peaked at day 16 in all the mesocosms except in M8, decreasing after one week. The class Gammaproteobacteria comprised between 20 to 45% of the total relative abundance. Within Gammaproteobacteria, the order Thiomicospirales had high relative abundance (8-17% total sequences) at day 10 in most of the mesocosms, whereas the order Cellvibrionales and order Oceanospirillales (genus *Pseudohongiella*) increased from day 24 and by the end of the experiment, respectively. In M8, the abundances of orders Thiomicospirales and Pseudomonadales (14% of total sequences) increased at day 24. Other groups that increased in abundance in the second half of the experiment were the deltaproteobacterial orders Desulfobacteriales (7-20% in M2, M3, M4 and M5) and Bdellovibrionales (5-8% in M2, M3 and M4). The order Flavobacteriales dominated within Bacteroidetes and the relative abundance ranged from 1 to 25% throughout the experiment, being generally high (10-20%) at day 10 . The flavobacterial genus *Aurantivirga* contributed > 7% in M1, M2 and M3.

Enzyme activity

The initial LAP activity before the OMZ-water addition was relatively low (average 359 nmol L^{-1} h^{-1} ± 81 nmol L^{-1} h^{-1} SD) but increased after the addition of OMZ-water in some of the mesocosms (Fig 6). In M3 the LAP activity was high, reaching 1600 nmol L^{-1} h^{-1} directly after

392 the OMZ-water addition, but decreased after that. The highest overall LAP activity throughout
393 the experiment was in M7 where the LAP activity was 716 nmol L^{-1} h^{-1} after OMZ-water
394 addition and the average after day 16 was 657 nmol L^{-1} h^{-1} ± 142 nmol L^{-1} h^{-1} (SD). There was a
395 slight difference between the treatments in the LAP activity after the addition of the OMZ-water
396 until day 16, with the very low OMZ signature (lowest NO_3 concentration) water producing the
397 highest LAP activity (Student's t-test, p = 0.047), but this difference disappeared after day 16 (p
398 = 0.44).

399 The alkaline phosphatase activity (APA) was 0.5-0.6 nmol L^{-1} h^{-1} at the beginning of the
400 experiment but decreased to undetectable levels after day 30 (Fig 7). There was a noticeable drop
401 in APA after the addition of the OMZ-water, and the decrease continued gradually until day 28
402 after which the APA was very low (<0.1 nmol L^{-1} d^{-1}). The APA was similar in all the
403 mesocosms and there was no treatment effect (p = 0.81). The exception to this was M3 where the
404 APA was lower, compared to all other mesocosms for most of the experiment (Fig 7).

405 The variability in APA was better explained by the measured variables than LAP (Fig 8). The
406 biogeochemical variables and bacterioplankton community separately explained 62% of the
407 variability in APA, whereas the phytoplankton community alone explained 57% of the
408 variability. Combining both the biogeochemical variables and the phytoplankton community
409 increased the explanatory power to 74% (bacterioplankton community not included as the
410 number of sample points were less). The variability in LAP activity was best explained by the
411 bacterioplankton community (38%) followed by biogeochemical variables (20%) and
412 phytoplankton community (18%). The combined biochemical variables and phytoplankton
413 community explained 28% of the LAP variability.

DISCUSSION

After the closure and addition of OMZ-water there was rapid phytoplankton growth in the upper 5 m of the mesocosms, with low light conditions limiting primary production deeper down (Bach et al., 2020). The DIN concentrations were depleted around day 18 coinciding with an increase in several of the FDOM components (both amino acid-like and humic-like components), also matching the end of the phytoplankton bloom. There was, however, relatively constant and low export of carbon out from the mesocosms (Bach et al., 2020) and at the same time relatively high Chl-*a* concentration (mostly >4 µg chl-*a* L^{-1}) under conditions with depleted DIN (Fig 3). In addition, the photochemical efficiency was overall relatively high (>0.5) throughout the experiment suggesting regenerated primary production driven by recycling of nutrients. The measured hydrolysis rates, particularly LAP, indicated that extracellular enzyme activity plays an important role for this recycled production.

The main aim of this study was to relate the biogeochemical and microbial community to the extracellular enzyme activity and a more detailed description of the temporal development and biomass comparison of microbial groups will be presented elsewhere in this special issue (e.g. Bach et al., 2020; Schulz et al 2021; Chen et al 2022; Paul et al 2022). Among phytoplankton, diatoms are typically dominating following upwelling events (Anabalón et al., 2016), whereas dinoflagellates tend to become more dominant after establishment of stratification (Margalef et al., 1979). This was also seen in our mesocosm as the dinoflagellate *Akashiwo sanguinea*, a mixotrophic species that may form red tides (Jeong et al., 2005; Badylak et al., 2014), which

quickly appeared in some mesocosms with some exceptions. In M3 it appeared a little later than in most mesocosms and in M4 it did not bloom at all. Interestingly these two mesocosms had a higher concentration of cryophytes and M4 had additionally a bloom event of picoeukaryotes. Being mixotrophic, *A. sanguinea* is known to prey on smaller species (Jeong et al., 2005) and lower grazing pressure could be the reason for the bloom of picoeukaryotes in M4.

The bacterial community composition changed during the experiment but without clear treatment effects. The dominant bacterial groups were the class Alphaproteobacteria, (Parvibaculales, SAR11 subclade Ia, Roseobacter clade and Rickettsiales), class Gammaproteobacteria (SAR116 clade, Cellvibrionales, Oceanospirillales and SUP05 clade) and to lesser extent the class Deltaproteobacteria (Desulfobacterales) and class Bacteroidea (order Flavobacteriales). SAR11 subclade Ia, Roseobacter clade, SAR116 clade, SUP05 clade and Desulfobacterales are known to utilize inorganic and organic sulfur components such as hydrogen sulfide (H_2S), sulfate (SO_4) and dimethylsulfoniopropionate (DMSP) metabolites for their metabolic requirements (Nowinski et al., 2019) and are coupled with the nitrogen cycle (Schunck et al., 2013). Specifically, the sulfur-oxidizing SPU05 oxidizes H_2S coupled with the nitrate reduction and potentially produces nitrite (Shah et al., 2017), whereas Desulfobacterales play an important role in N_2 fixation (Gier et al., 2016). These bacterial taxa associated with the sulfur cycle are typically found in the OMZ regions (Pajares et al., 2020). We observed a temporal shift in the bacterial community through the experiment changing between sulfur-oxidizing (SUP05) and sulfate-reducing (Desulfobacterales) bacteria, probably linked to the nitrate availability, i.e. more DIN at the enclose of the mesocosms and thus more relative abundance of SUP05. We also observed a shift within phytoplankton-associated bacteria (*Roseobacter* lineage, Gammaproteobacteria, and Flavobacteriales) that likely responded to the availability of DOM supply during the experiment

(Buchan et al 2014, Chafee et al 2017). The high relative abundance of Flavobacteriales and genera from the *Roseobacter* lineage on days 10 and 16, respectively, coincided with the increase in chl-*a* and high LAP activity until day 16. Positive correlations have been observed between chl-*a*, Bacteroides and Deltaproteobacteria and LAP during phytoplankton blooms (Shi et al 2019). However, we do not have gene expression data and cannot make any firm conclusion about the connection between these groups and production of LAP.

The temporal shift in the bacterial community indicates niche partitioning between bacterial taxa that assimilate different organic substrates or inorganic sulfur components, produced during phytoplankton bloom events or from sulfidic events (Schunck et al., 2013; Callbeck et al., 2018; Nowinski et al., 2019). Our results support previous studies that have demonstrated the important role of the sulfur cycle in shaping the bacterial community composition in poorly oxygenated waters (Schunck et al., 2013; Aldunate et al., 2018). It is worth noting that the conditions in the bottom of the mesocosms were sub-oxic and there might have been a clear depth gradient in the bacterial community that was not picked up by our integrated 0-10 m sampling.

Overall, there was a treatment effect of the different OMZ waters on the LAP activity, with higher LAP in the very low OMZ signature addition, but this effect was only observed right after the addition of the OMZ-water. There were also slightly higher NO_3 concentrations in this water (Bach et al., 2020). However, this difference in both DIN and LAP was relatively small and disappeared a week after the OMZ water addition, most likely because the collected OMZ-water was more similar between the two locations than anticipated, with relatively similar concentrations of DIN. Although there were differences between individual mesocosms in terms of the plankton community structure, there were no clear differences between treatments, and we can conclude that the availability of nutrients by itself can shift the LAP production.

The LAP activity in our study was very high (~10-times higher compared with most literature data). In a comparable study but further offshore in Peru, the LAP activity was 20 – 65 nmol L^{-1} h^{-1} in surface waters (Maßmig et al., 2020). Further to the south, in Chile (30° 30.80' S), values up to 230 nmol L^{-1} h^{-1} have been recorded, with a clear seasonal cycle linked to upwelling events (Gutiérrez et al., 2011). With most of our data ranging between 200 – 800 nmol L^{-1} h^{-1} it is clear that these LAP activities are linked to the upwelling, which is more intense near the coast and also more constant at the study site compared with sites further south. The enzyme activity in sediments can be up to three orders of magnitude higher than what we found (Hoppe et al., 2002), and an order of magnitude higher values have been observed in a eutrophic, salt-water lake (Song et al., 2019). The high LAP activities are likely a reflection of the high microbial activity in the Peruvian upwelling system. The experiment was also taking place during a rare coastal El Niño event (Garreaud, 2018), with anomalous higher surface temperatures (20-22 °C), which could be a reason for the high values we recorded as LAP activity is known to increase with temperature (Christian and Karl, 1995).

There was also some loss of N due to denitrification, estimated to 0.2-4.2 nmol N_2 L^{-1} h^{-1} during the experiment (Schulz et al 2021). For comparison, the LAP activity suggested an average of 417 nmol L^{-1} h^{-1} hydrolyzation of N-containing compounds, but this should be seen as the maximal potential rather than the actual rate. The use of fluorescently labelled substrates for measuring extracellular activity is a proxy method that has some drawbacks. The primary one is that the molecular structure of the substrate used is never equivalent to the high molecular weight DOM in the water. This means that the measured hydrolysis rates could be an overestimation of the actual hydrolysis rates of DOM (e.g. Arnosti, 2011). The primary benefit of the method is that it is straightforward and has been in widespread use for decades, which means that

505 comparisons with other ecosystems is possible, and for our purpose, we use it for better
506 understanding how much of the variability can be explained by the other measured variables.

507 Considering the APA, the most interesting aspect was that it was measurable in the beginning of
508 the experiment at high PO_4^{3-} concentration. This high APA activity at high PO_4^{3-} concentration
509 has been observed in deep oceans (Hoppe and Ullrich, 1999; Baltar et al 2016). Baltar et al.
510 (2016) also observed an increase in APA in experiments amended with organic matter
511 suggesting the activity of APA was linked to organic matter supply, independently of the PO_4^{3-}
512 concentration. This could be due to bacterial APA, which is more complex than for
513 phytoplankton, in that it can be linked to the hydrolysis and acquisition of C (Hoppe, 2003). In
514 our experiment, the initial decrease in DOP and increase in PO_4^{3-} concentrations indicates that P
515 released by AP hydrolysis was added to the PO_4^{3-} pool. This suggests that APA was not used for
516 P acquisition.

517 It is known that APA stays suspended and active for a long time in marine environments, and
518 cell-free APA was reduced by only 25% over 16 days in the experiment by Thomson et al.
519 (2019). If this enzyme is viable for this long, it suggests that there was no new production of AP
520 after the closure of the mesocosms, which is supported by the dilution effect of adding the OMZ-
521 water. In that case, the disappearance of the initial AP took 30 days.

522 The hydrolysis rates of AP were relatively low compared with most published data, probably
523 linked to the clear surplus of PO_4^{3-}. It is worth noting, however, that we were most likely not
524 measuring the maximal potential hydrolysis rates as substrate addition was relatively low (100
525 nmol L^{-1}) and would likely have been higher with more added substrate. This could be the reason
526 for the apparent discrepancy between the measured hydrolysis rates and the change in the PO_4^{3-}

and DOP pools during the 10 first days of the experiment. During this time there was a decrease of approximately 0.5 µmol DOP L^{-1} and an increase of 0.6 µmol PO_4^{3-} L^{-1}, suggesting an actual hydrolysis rate of 2.0-2.5 nmol L^{-1} h^{-1} (assuming 500-600 nmol over 10 days). This is a factor 3-4 higher compared with the initially measured APA of ~0.6 nmol L^{-1} h^{-1}.

The statistical model that we applied was better at explaining the variability in APA compared with the LAP activity. APA gradually decreased during the initial phase of the experiment to undetectable levels after the middle of the experiment. Any correlation does not mean causality and the higher coefficient of determination is probably rather a reflection of the clear temporal development in APA. If the AP was produced before the closure of the mesocosm and slowly degraded as discussed above, any connection with the biogeochemical or plankton community was likely due to unrelated temporal development; for example, the DIN also decreased over time.

For the LAP activity the overall explanatory power by the biogeochemical and plankton community composition was less than for APA, but interestingly the bacterioplankton community composition clearly explained the variability better (38%) than the combined biogeochemical and phytoplankton community (28%). Considering that the bacterial community was not sampled as frequently as the biogeochemical variables and flow cytometer counts, we suspect that the explanatory power would have increased with more frequent sampling. It is likely that bacteria were producing the LAP activity and some taxa are more reliant on enzyme production for nutrient acquisition than others (Ramin and Allison, 2019). Some dinoflagellates are also known to produce LAP and most of the mesocosms with high dinoflagellate biomass except M4. However, the phytoplankton community only explained 18% of the variability in

549 LAP activity, and these dinoflagellates were likely not producing any substantial amount of this
550 enzyme.

551 In conclusion, there was measurable APA at the start of the experiment, but this gradually
552 declined to undetectable levels in all the mesocosms midway (~30 days) in the experiment. With
553 high concentrations of PO_4^{3-}, low APA is not surprising, and AP is a relatively slowly degrading
554 enzyme that could have been fully dissolved and produced before the closure of the mesocosms.
555 Our statistical model explained better the variability of APA (74%) compared with LAP activity,
556 probably due to the clear temporal development of APA that was likely independent of some of
557 the other temporal trends such as decreasing DIN. We found very high levels of LAP activity
558 (mostly in the range 200 – 800 nmol L^{-1} h^{-1}), which is an order of magnitude higher than most
559 literature data. This is probably linked to the upwelling supporting high levels of microbial
560 activity in combination with the general DIN limitation in the coastal Peruvian upwelling. The
561 bacterioplankton community composition explained best the variability of LAP activity (38%)
562 compared with the combined biochemical and phytoplankton community model (28%). With
563 more than 50% of the variability unaccounted for, we are still missing important pieces of the
564 puzzle understanding the variability in LAP activity. The high hydrolysis rates for LAP suggests
565 that pelagic N remineralization supported the relatively high standing stock of primary producers
566 (mostly >4 µg chl-*a* L^{-1}) in the mesocosms after N depletion.

567

568

569 Data availability

All data will be made available on the permanent repository www.pangaea.de after publication.

The DNA sequencing data will be submitted to NCBI SRA (in prep).

Author contribution

Samples were taken by KS, JP, JA, LB, EvdE, MF, NHH, JM and UR. In addition to the sampling crew, further data analysis was conducted by MTCG and MGL. UR developed the experimental design and sampling strategy and coordinated the mesocosm campaign. All co-authors contributed to the data interpretation. KS wrote the manuscript with contributions from all co-authors.

ACKNOWLEDGEMENTS

The experiment was funded through the German Research Foundation (DFG) project: Collaborative Research Centre SFB 754 Climate1074 Biogeochemistry Interactions in the Tropical Ocean. Additional funding came from the Academy of Finland (decision 259164; KS and JP), the EU project AQUACOSM (UR) under grant No. 731065 of the European Union's Horizon 2020 research and innovation programme, the Leibniz Award 2012 of the German Research Foundation (UR) and the Helmholtz International Fellow Award 2015 (JA). This study also used SYKE marine research infrastructure as a part of the Finnish FINMARI consortium. The publication of sequencing data was approved by the Peruvian Ministry of Production with respect to the access and benefit sharing regulations of the Nagoya protocol.

We thank all participants of the KOSMOS-Peru 2017 study for assisting in mesocosm sampling and maintenance in particular: Andrea Ludwig, Jana Meyer, Jean-Pierre Bednar, Gabriela Chavez, Susanne Feiersinger, Peter Fritsche, Paul Stange, Anna Schukat and Michael Krudewig. We are particularly thankful to the staff of IMARPE for their support during the planning, and to the Marina de Guerra del Perú, the Dirección General de Capitanías y Guardacostas and the Club Náutico Del Centro Naval for their great support. The NMDS plots and GAM models were produced by Dr. Riina Klais-Peets at EcoStat ltd.

REFERENCES

Aldunate, M., De la Iglesia, R., Bertagnolli, A. D., and Ulloa, O.: Oxygen modulates bacterial community composition in the coastal upwelling waters off central Chile, Deep Sea Research Part II: Topical Studies in Oceanography, 156, 68-79, 2018.

Ammerman, J.: Microbial cycling of inorganic and organic phosphorus in the water column, Handbook of methods in aquatic microbial ecology, 1, 649-660, 1993.

Anabalón, V., Morales, C., González, H., Menschel, E., Schneider, W., Hormazabal, S., Valencia, L., and Escribano, R.: Micro-phytoplankton community structure in the coastal upwelling zone off Concepción (central Chile): Annual and inter-annual fluctuations in a highly dynamic environment, Prog Oceanogr, 149, 174-188, 2016.

609 Arnosti, C.: Microbial extracellular enzymes and the marine carbon cycle, Ann Rev Mar Sci, 3,
610 401-425, 2011.

611 Bach, L. T., Alvarez-Fernandez, S., Hornick, T., Stuhr, A., and Riebesell, U.: Simulated ocean
612 acidification reveals winners and losers in coastal phytoplankton, PloS one, 12, e0188198, 2017.

613 Bach, L. T., Paul, A. J., Boxhammer, T., Esch, E. v. d., Graco, M., Schulz, K. G., Achterberg, E.,
614 Aguayo, P., Aristegui, J., Ayon, P., Banos, I., Bernales, A., Boegeholz, A. S., Chavez, F., Chen,
615 S.-M., Doering, K., Filella, A., Fischer, M., Grasse, P., Haunost, M., Hennke, J., Hernandez-
616 Hernandez, N., Hopwood, M., Igarza, M., Kalter, V., Kittu, L., Kohnert, P., Ledesma, J.,
617 Lieberum, C., Lischka, S., Loescher, C., Ludwig, A., Mendoza, U., Meyer, J., Meyer, J.,
618 Minutolo, F., Cortes, J. O., Piiparinen, J., Sforna, C., Spilling, K., Sanchez, S., Spisla, C., Sswat,
619 M., Moreira, M. Z., and Riebesell, U.: Factors controlling plankton productivity, particulate
620 matter stoichiometry, and export flux in the coastal upwelling system off Peru, Biogeosciences
621 17: 4831-4852, 2020.

622 Badylak, S., Phlips, E. J., and Mathews, A. L.: Akashiwo sanguinea (Dinophyceae) blooms in a
623 sub-tropical estuary: an alga for all seasons, Plankt Benthos Res, 9, 147-155, 2014.

624 Barlow, R., Cummings, D., and Gibb, S.: Improved resolution of mono-and divinyl chlorophylls
625 a and b and zeaxanthin and lutein in phytoplankton extracts using reverse phase C-8 HPLC, Mar
626 Ecol Prog Ser, 161, 303-307, 1997.

627 Benitez-Nelson, C. R., and Buesseler, K. O.: Variability of inorganic and organic phosphorus
628 turnover rates in the coastal ocean, Nature, 398, 502-505, 1999.

Bolger, A. M., Lohse, M., and Usadel, B.: Trimmomatic: a flexible trimmer for Illumina sequence data, Bioinformatics, 30, 2114-2120, 2014.

Buchan, A., G. R. LeCleir, C. A. Gulvik, and J. M. González. 2014. Master recyclers: Features and functions of bacteria associated with phytoplankton blooms. Nat. Rev. Microbiol. 12: 686–698. doi:10.1038/nrmicro3326.

Burley, S. K., David, P. R., Taylor, A., and Lipscomb, W. N.: Molecular structure of leucine aminopeptidase at 2.7-A resolution, Proc Natl Acad Sci, 87, 6878-6882, 1990.

Canfield D., Kristensen E., and Thamdrup B.: Aquatic geomicrobiology. Elsevier, 2005.

Callbeck, C. M., Lavik, G., Ferdelman, T. G., Fuchs, B., Gruber-Vodicka, H. R., Hach, P. F., Littmann, S., Schoffelen, N. J., Kalvelage, T., and Thomsen, S.: Oxygen minimum zone cryptic sulfur cycling sustained by offshore transport of key sulfur oxidizing bacteria, Nature Com, 9, 1-11, 2018.

Chafee M, Fernàndez-Guerra A, Buttigieg PL, Gerdts G, Eren AM, Teeling H, Amann RI (2017) Recurrent patterns of microdiversity in a temperate coastal marine environment. The ISME J 12:237

Chavez, F. P., Bertrand, A., Guevara-Carrasco, R., Soler, P., and Csirke, J.: The northern Humboldt Current System: Brief history, present status and a view towards the future, Prog Oceanogr, 79, 95-105, 2008.

Chen, S.-M., Riebesell, U., Schulz, K. G., von der Esch, E., Achterberg, E. P., and Bach, L. T.: Temporal dynamics of surface ocean carbonate chemistry in response to natural and simulated

upwelling events during the 2017 coastal El Niño near Callao, Peru, Biogeosciences, 19, 295–312, 2022.

Christian J.R., Karl D.M.: Bacterial ectoenzymes in marine waters: activity ratios and temperature responses in three oceanographic provinces. Limnol Oceanogr, 40:1042-1049, 1995.

Coverly, S., Kérouel, R., and Aminot, A.: A re-examination of matrix effects in the segmented-flow analysis of nutrients in sea and estuarine water, Analytica chimica acta, 712, 94-100, 2012.

Edgar, R. C., Haas, B. J., Clemente, J. C., Quince, C., and Knight, R.: UCHIME improves sensitivity and speed of chimera detection, Bioinformatics, 27, 2194-2200, 2011.

Ewing, B., and Green, P.: Base-calling of automated sequencer traces using phred. II. Error probabilities, Genome Res, 8, 186-194, 1998.

Ewing, B., Hillier, L., Wendl, M. C., and Green, P.: Base-calling of automated sequencer traces usingPhred. I. Accuracy assessment, Genome Res, 8, 175-185, 1998.

FAO: The state of world fisheries and aquaculture, Food and Agriculture Organization of the United Nations, Rome, 223 pp., 2018.

Fischer, M. A., Güllert, S., Refai, S., Künzel, S., Deppenmeier, U., Streit, W. R., and Schmitz, R. A.: Long-term investigation of microbial community composition and transcription patterns in a biogas plant undergoing ammonia crisis, Microb Biotechnol, 12, 305-323, 2019a.

Fischer, M. A., Ulbricht, A., Neulinger, S. C., Refai, S., Waßmann, K., Künzel, S., and Schmitz-Streit, R. A.: Immediate effects of ammonia shock on transcription and composition of a biogas reactor microbiome, Front Microbiol, 10, 2064, 2019b.

669 Garreaud, R. D.: A plausible atmospheric trigger for the 2017 coastal El Niño, International J
670 Climatol, 38, e1296-e1302, 2018.

671 Gier, J., Sommer, S., Löscher, C. R., Dale, A. W., Schmitz-Streit, R., and Treude, T.: Nitrogen
672 fixation in sediments along a depth transect through the Peruvian oxygen minimum zone,
673 Biogeosciences, 13, 4065-4080, 2016.

674 Graco, M. I., Purca, S., Dewitte, B., Castro, C. G., Morón, O., Ledesma, J., Flores, G., and
675 Gutiérrez, D.: The OMZ and nutrient features as a signature of interannual and low-frequency
676 variability in the Peruvian upwelling system, Biogeosciences, 14, 4601-4617, 2017.

677 Gutiérrez, M., Pantoja, S., Tejos, E., and Quiñones, R.: The role of fungi in processing marine
678 organic matter in the upwelling ecosystem off Chile, Mar Biol, 158, 205-219, 2011.

679 Hauss, H., Franz, J. M., and Sommer, U.: Changes in N: P stoichiometry influence taxonomic
680 composition and nutritional quality of phytoplankton in the Peruvian upwelling, J Sea Res, 73,
681 74-85, 2012.

682 Hoppe, H.-G., Kim, S.-J., and Gocke, K.: Microbial decomposition in aquatic environments:
683 combined process of extracellular enzyme activity and substrate uptake, Appl. Environ.
684 Microbiol., 54, 784-790, 1988.

685 Hoppe, H.-G., Arnosti, C., and Herndl, G.: Ecological significance of bacterial enzymes in the
686 marine environment, in: Enzymes in the Environment: Activity, Ecology, and Applications,
687 edited by: Burns R. G and Dick R. P), Marcel Dekker, New York, 73-107, 2002.

688 Hoppe, H.-G.: Phosphatase activity in the sea, Hydrobiol, 493, 187-200, 2003.

689 Jeong, H. J., Du Yoo, Y., Park, J. Y., Song, J. Y., Kim, S. T., Lee, S. H., Kim, K. Y., and Yih,
690 W. H.: Feeding by phototrophic red-tide dinoflagellates: five species newly revealed and six
691 species previously known to be mixotrophic, Aquat Microb Ecol, 40, 133-150, 2005.

692 Kalvelage, T., Lavik, G., Lam, P., Contreras, S., Arteaga, L., Löscher, C. R., Oschlies, A.,
693 Paulmier, A., Stramma, L., and Kuypers, M. M.: Nitrogen cycling driven by organic matter
694 export in the South Pacific oxygen minimum zone, Nature Geosci, 6, 228-234, 2013.

695 Keeling, R. F., Körtzinger, A., and Gruber, N.: Ocean deoxygenation in a warming world, Ann
696 Rev Mar Sci, 2, 199-229, 2010.

697 Kérouel, R., and Aminot, A.: Fluorometric determination of ammonia in sea and estuarine waters
698 by direct segmented flow analysis, Mar Chem, 57, 265-275, 1997.

699 Labry, C., Delmas, D., Youenou, A., Quere, J., Leynaert, A., Fraisse, S., Raimonet, M., and
700 Ragueneau, O.: High alkaline phosphatase activity in phosphate replete waters: The case of two
701 macrotidal estuaries, Limnol Oceanogr, 61, 1513-1529, 2016.

702 Margalef, R., Estrada, M., and Blasco, D.: Functional morphology of organisms involved in red
703 tides, as adapted to decaying turbulence, in: Toxic dinoflagellate blooms, edited by: Taylor, D.
704 L., and Seliger, H. H., Elsevier-North Holland, Amsterdam, 89-94, 1979.

705 Maßmig, M., Lüdke, J., Krahmann, G., and Engel, A.: Bacterial degradation activity in the
706 eastern tropical South Pacific oxygen minimum zone, Biogeosciences, 17, 215-230, 2020.

707 Messié, M., and Chavez, F. P.: Seasonal regulation of primary production in eastern boundary
708 upwelling systems, Prog Oceanogr, 134, 1-18, 2015.

709 Morris, A., and Riley, J.: The determination of nitrate in sea water, Analytica Chimica Acta, 29,
710 272-279, 1963.

711 Murphy, J., and Riley, J. P.: A modified single solution method for the determination of
712 phosphate in natural waters, Analytica Chimica Acta, 27, 31-36, 1962.

713 Murphy, K. R., Stedmon, C. A., Wenig, P., and Bro, R.: OpenFluor–an online spectral library of
714 auto-fluorescence by organic compounds in the environment, Analytical Meth, 6, 658-661, 2014.

715 Nausch, M.: Alkaline phosphatase activities and the relationship to inorganic phosphate in the
716 Pomeranian Bight (southern Baltic Sea), Aquat Microb Ecol, 16, 87-94, 1998.

717 Nowinski, B., Motard-Côté, J., Landa, M., Preston, C. M., Scholin, C. A., Birch, J. M., Kiene, R.
718 P., and Moran, M. A.: Microdiversity and temporal dynamics of marine bacterial
719 dimethylsulfoniopropionate genes, Env Microbiol, 21, 1687-1701, 2019.

720 Oksanen, J., Blanchet, F.G., Kindt, R., Legendre, P.M.P.R., Minchin, P.R., O'hara, R.B.,
721 Simpson, G., Solymos, P., Henry, M. and Stevens, H.: Ordination methods, diversity analysis
722 and other functions for community and vegetation ecologists, Vegan: Community Ecol Package,
723 5-26, 2017. Oschlies, A., Brandt, P., Stramma, L., and Schmidtko, S.: Drivers and mechanisms
724 of ocean deoxygenation, Nature Geosci, 11, 467-473, 2018.

725 Pajares, S., Varona-Cordero, F., and Hernández-Becerril, D. U.: Spatial Distribution Patterns of
726 Bacterioplankton in the Oxygen Minimum Zone of the Tropical Mexican Pacific, Microb Ecol,
727 2020.

Paul, A. J., Bach, L. T., Arístegui, J., von der Esch, E., Hernández-Hernández, N., Piiparinen, J., Ramajo, L., Spilling, K., and Riebesell, U.: Upwelled plankton community modulates surface bloom succession and nutrient availability in a natural plankton assemblage, Biogeosciences, 19, 5911–5926, 2022.

Perry, M.: Alkaline phosphatase activity in subtropical Central North Pacific waters using a sensitive fluorometric method, Mar Biol, 15, 113-119, 1972.

Pruesse, E., Peplies, J., and Glöckner, F. O.: SINA: accurate high-throughput multiple sequence alignment of ribosomal RNA genes, Bioinformatics, 28, 1823-1829, 2012.

Rose, C., and Axler, R. P.: Uses of alkaline phosphatase activity in evaluating phytoplankton community phosphorus deficiency, Hydrobiol, 361, 145-156, 1997.

Ramin K.I., and Allison S.D.: Bacterial tradeoffs in growth rate and extracellular enzymes. Front Microbiol, 10: 2956, 2019.

Schloss, P. D., Westcott, S. L., Ryabin, T., Hall, J. R., Hartmann, M., Hollister, E. B., Lesniewski, R. A., Oakley, B. B., Parks, D. H., and Robinson, C. J.: Introducing mothur: open-source, platform-independent, community-supported software for describing and comparing microbial communities, Appl Env Microbiol, 75, 7537-7541, 2009.

Schulz, K. G., Achterberg, E. P., Arístegui, J., Bach, L. T., Baños, I., Boxhammer, T., Erler, D., Igarza, M., Kalter, V., Ludwig, A., Löscher, C., Meyer, J., Meyer, J., Minutolo, F., von der Esch, E., Ward, B. B., and Riebesell, U.: Nitrogen loss processes in response to upwelling in a Peruvian coastal setting dominated by denitrification – a mesocosm approach, Biogeosciences, 18, 4305–4320, 2021.

749 Schunck, H., Lavik, G., Desai, D. K., Großkopf, T., Kalvelage, T., Löscher, C. R., Paulmier, A.,
750 Contreras, S., Siegel, H., and Holtappels, M.: Giant hydrogen sulfide plume in the oxygen
751 minimum zone off Peru supports chemolithoautotrophy, PloS One, 8, e68661, 2013.

752 Shah, V., Chang, B. X., and Morris, R. M.: Cultivation of a chemoautotroph from the SUP05
753 clade of marine bacteria that produces nitrite and consumes ammonium, ISME J, 11, 263-271,
754 2017.

755 Song, C., Cao, X., Zhou, Y., Azzaro, M., Monticelli, L. S., Maimone, G., Azzaro, F., La Ferla,
756 R. and Caruso, G.: Nutrient regeneration mediated by extracellular enzymes in water column and
757 interstitial water through a microcosm experiment. Sci Tot Env 670, 982-992, 2019.

758 Spilling, K., Camarena-Gómez, M.-T., Lipsewers, T., Martinez-Varela, A., Díaz-Rosas, F.,
759 Eronen-Rasimus, E., Silva, N., von Dassow, P., and Montecino, V.: Impacts of reduced inorganic
760 N: P ratio on three distinct plankton communities in the Humboldt upwelling system, Mar Biol,
761 166, 114, 2019.

762 Steen, A.D., Vazin, J.P., Hagen, S.M., Mulligan, K.H. and Wilhelm, S.W.: Substrate specificity
763 of aquatic extracellular peptidases assessed by competitive inhibition assays using synthetic
764 substrates, Aquat Microb Ecol, 75, 271-281, 2015.

765 Stedmon, C. A., and Bro, R.: Characterizing dissolved organic matter fluorescence with parallel
766 factor analysis: a tutorial, Limnology and Oceanography: Methods, 6, 572-579, 2008.

767 Stoecker, D. K., and Gustafson, D. E.: Cell-surface proteolytic activity of photosynthetic
768 dinoflagellates, Aquat Microb Ecol, 30, 175-183, 2003.

769 Thomson, B., Wenley, J., Currie, K., Hepburn, C., Herndl, G. J., and Baltar, F.: Resolving the
770 paradox: continuous cell-free alkaline phosphatase activity despite high phosphate
771 concentrations, Mar Chem, 214, 103671, 2019.

772 Wood, S. N.: Generalized additive models: an introduction with R, CRC press, New York, 2017.

773

774

775

776

777 Figure legends

778

779 Fig 1. The concentration of dissolved inorganic nitrogen (DIN), phosphate (PO_4^{3-}), dissolved
780 organic nitrogen (DON) and phosphorus (DOP). The red and blue color are the mesocosm bags
781 with addition of water with low (closer to shore) and very low (further offshore) oxygen
782 minimum zone (OMZ) signature, respectively. The green dashed lines denote the time of OMZ
783 water addition. Pacific denotes measurements from water collected next to, but outside of the
784 mesocosms.

785

786 Fig 2. The fluorescence dissolved organic matter (FDOM) components (C1-C4) during the
787 experiment. The red and blue color are the mesocosm bags with addition of water with low

(closer to shore) and very low (further offshore) oxygen minimum zone (OMZ) signature, respectively. The green dashed lines denote the time of OMZ water addition. Pacific denotes measurements from water collected next to, but outside of the mesocosms.

Fig 3. The Chlorophyll-*a* (Chl-*a*) concentration (upper graph) and the photochemical efficiency (lower graph). The red and blue color are the mesocosm bags with addition of water with low (closer to shore) and very low (further offshore) oxygen minimum zone (OMZ) signature, respectively. The green dashed lines denote the time of OMZ water addition. Pacific denotes measurements from water collected next to, but outside of the mesocosms.

Fig 4. Development of the main groups of phytoplankton enumerated by flow cytometry. The red and blue color are the mesocosm bags with addition of water with low (closer to shore) and very low (further offshore) oxygen minimum zone (OMZ) signature, respectively. The green dashed lines denote the time of OMZ water addition. Pacific denotes measurements from water collected next to, but outside of the mesocosms.

Fig 5. The bacterial community composition in the 8 mesocosms taken at different time points. In the upper row are mesocosms with water from low OMZ signature (30 m depth) and in the second row with very low OMZ signature (70 m depth). The Y-axis indicates the relative abundance of the bacterial taxa. Only the groups that contributed more than 0.5 % of the total sequences are included and the rest are grouped as “Other Bacteria”. The classification was

809 performed mainly in class, order and genus levels. The abbreviations indicate the main class
810 levels: Alphaproteobacteria (orange shades), Gammaproteobacteria (blue-pink shades),
811 Deltaproteobacteria (green shades), and Bacteroidia (yellow shades) .

812

813 Fig 6. The leucine aminopeptidase (LAP) activity. The red and blue color are the mesocosm bags
814 with addition of water with low (closer to shore) and very low (further offshore) oxygen
815 minimum zone (OMZ) signature, respectively. The green dashed lines denote the time of OMZ
816 water addition. Pacific denotes measurements from water collected next to, but outside of the
817 mesocosms.

818

819 Fig 7. The alkaline phosphatase activity (APA). The red and blue color are the mesocosm bags
820 with addition of water with low (closer to shore) and very low (further offshore) oxygen
821 minimum zone (OMZ) signature, respectively. The green dashed lines denote the time of OMZ
822 water addition.

823

824 Fig 8. Non-parametric multidimensional scaling (NMDS) plots for biochemical, phytoplankton
825 community and bacterioplankton community (upper row). From the NMDS scores, generalized
826 additive models (GAMs) were made (lower two rows) where we used alkaline phosphatase
827 activity (APA) and leucine aminopeptidase (LAP) as dependent variables. The output scores
828 (mds1 and mds2) of the NMDS are depicted in the lower two rows.

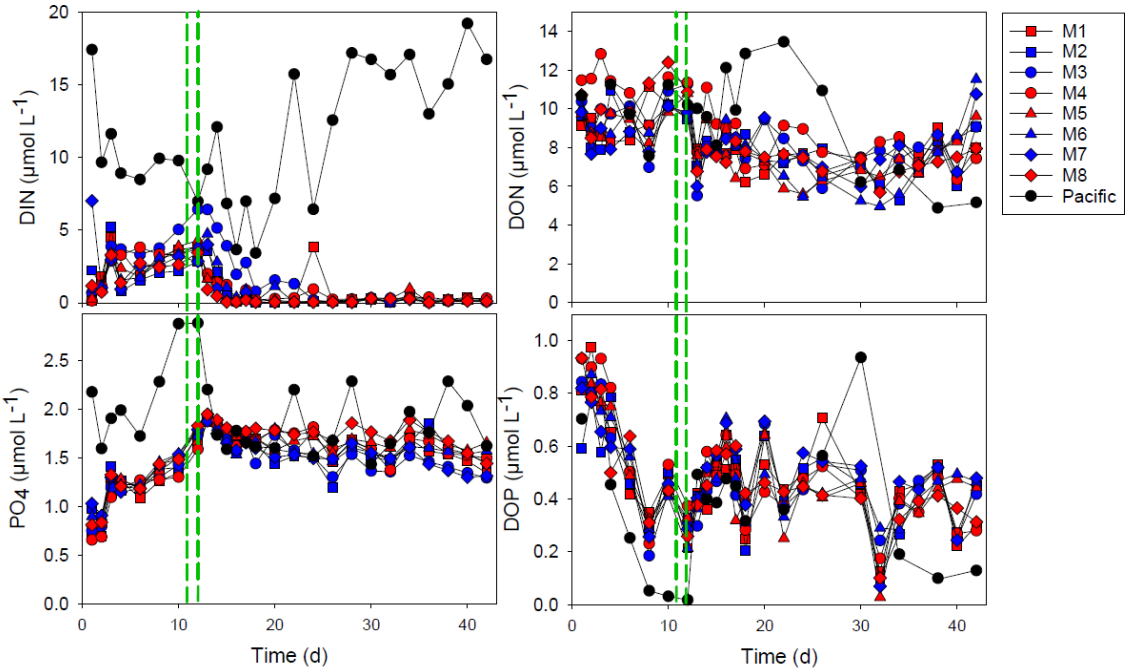

FIG 1

829
830
831
832

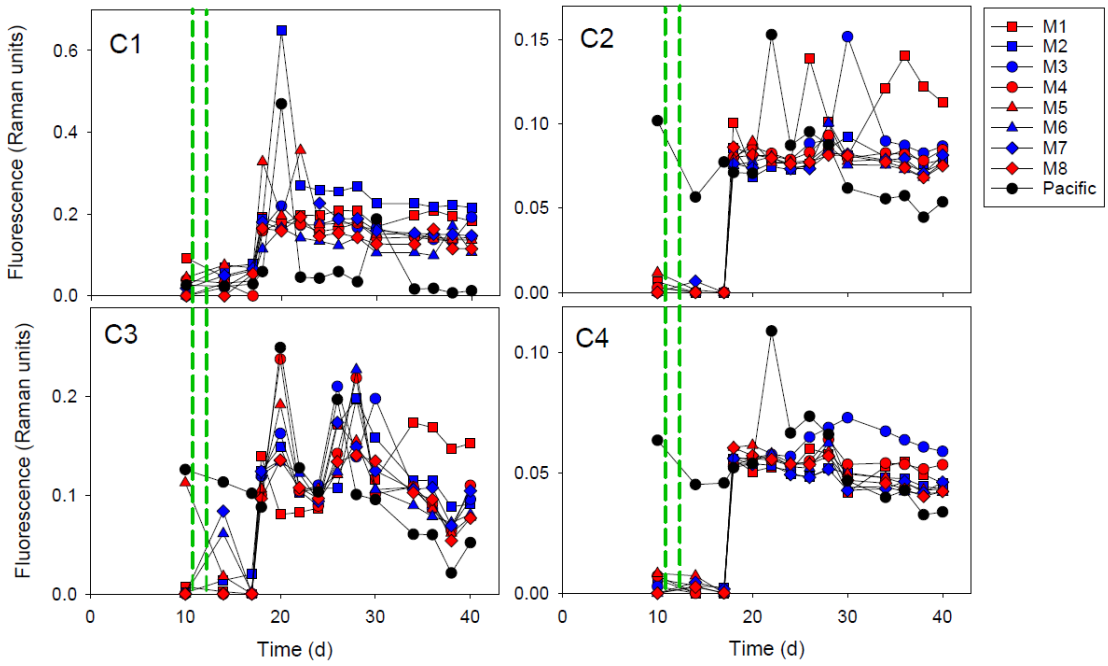
C1
C2
C3
C4
Fluorescence (Raman units)
Fluorescence (Raman units)
Time (d)
Time (d)
M1
M2
M3
M4
M5
M6
M7
M8
Pacific

FIG 2

833
834

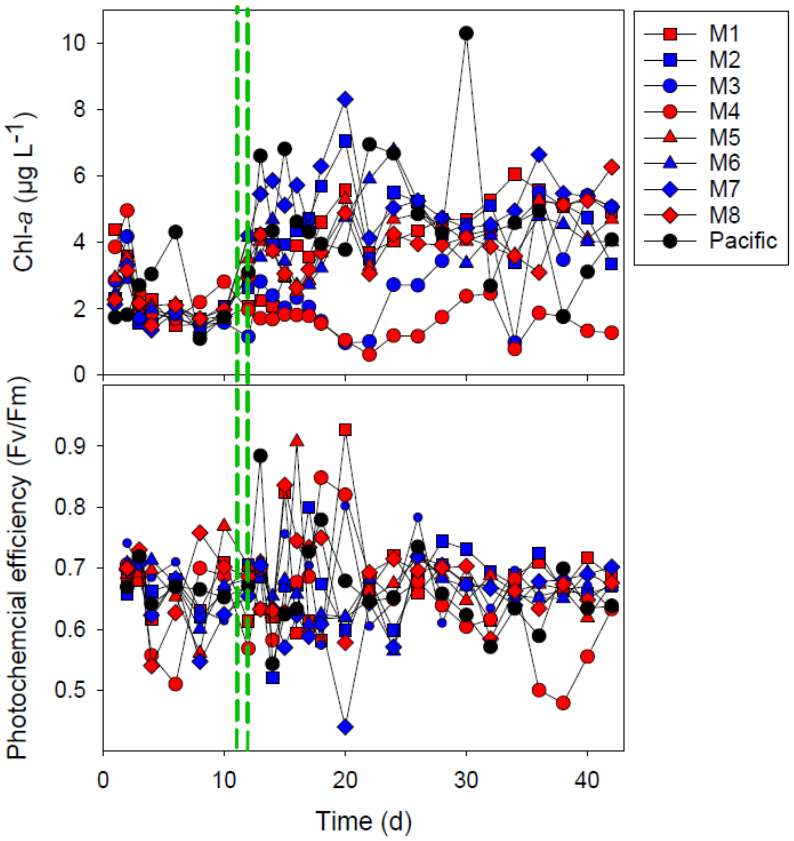
Chl-a (µg L-1)
Photochemcial efficiency (Fv/Fm)
Time (d)
M1
M2
M3
M4
M5
M6
M7
M8
Pacific

FIG 3

835
836

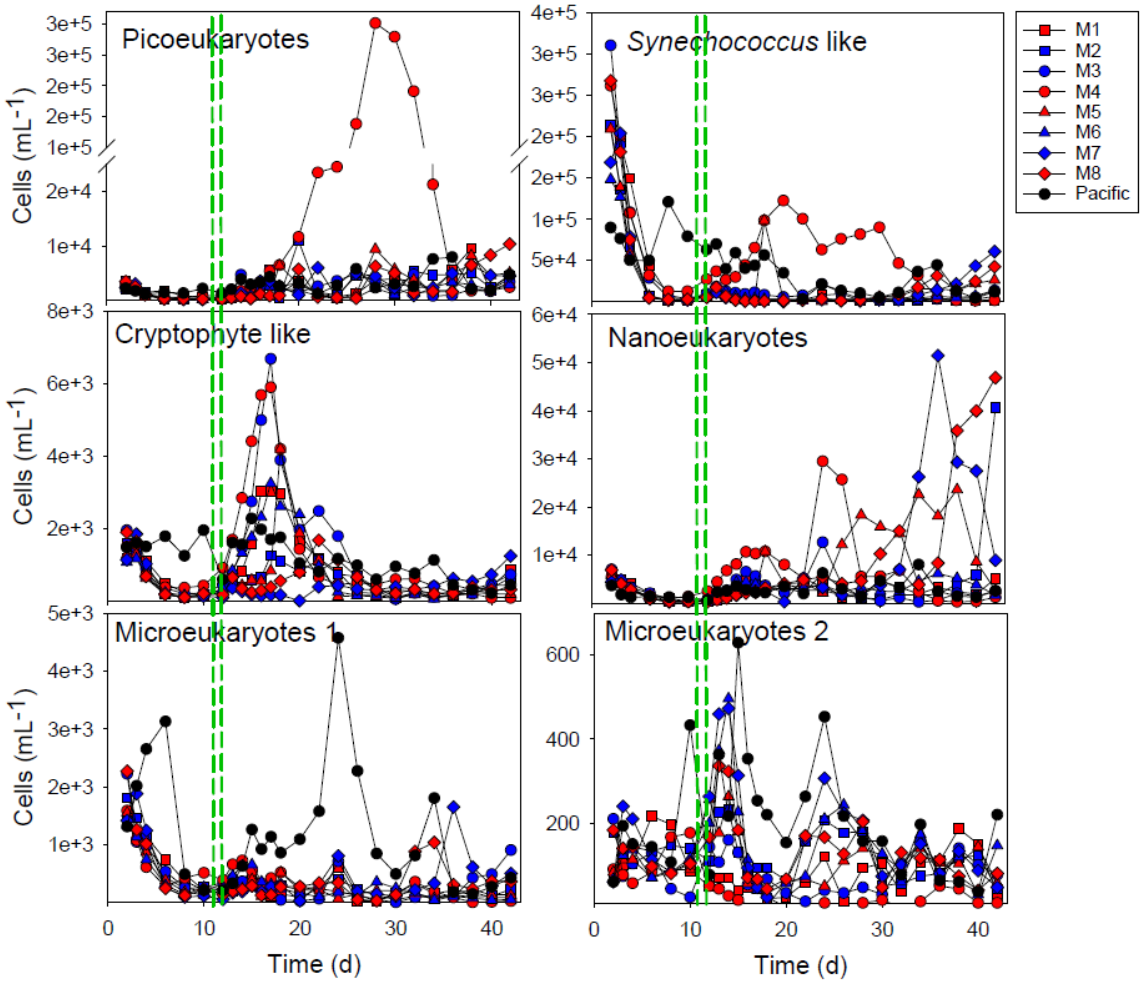
Picoeukaryotes
Synechococcus like
Cryptophyte like
Nanoeukaryotes
Microeukaryotes 1
Microeukaryotes 2
Cells (mL-1)
Time (d)
M1
M2
M3
M4
M5
M6
M7
M8
Pacific

FIG 4

840

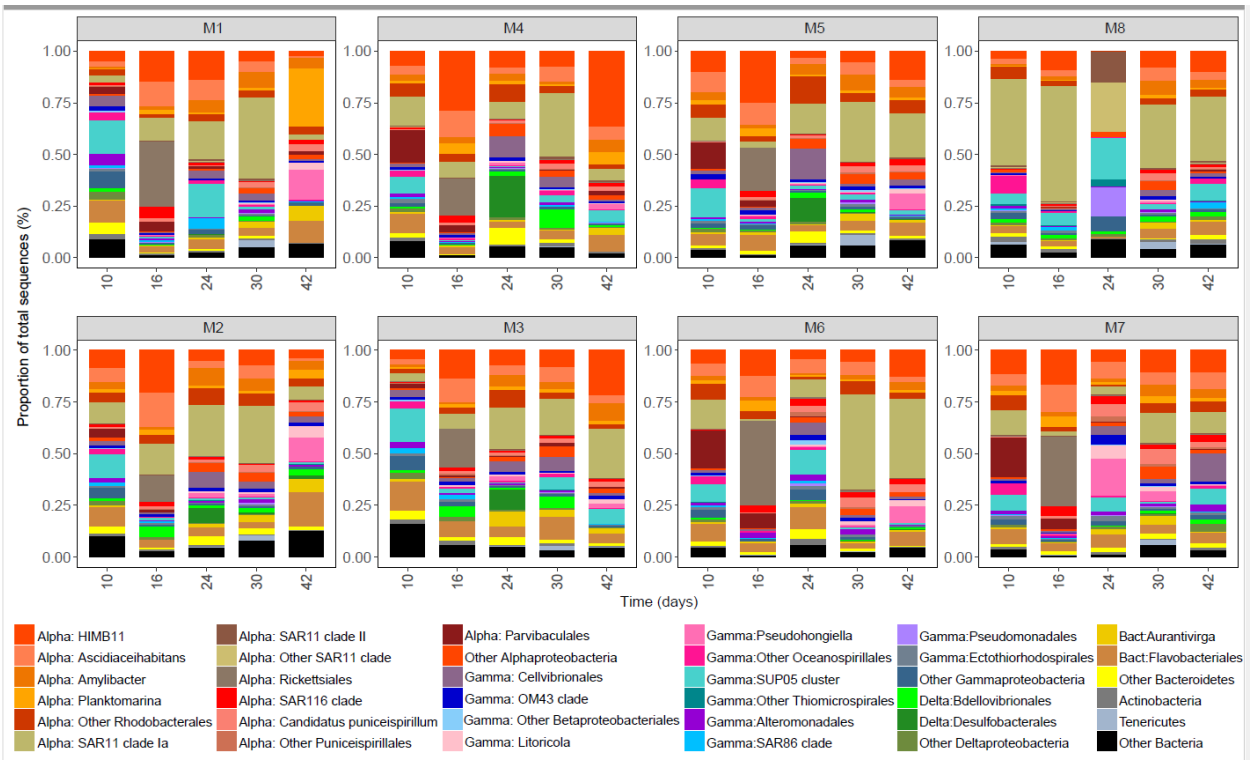

841

842 FIG 5

843

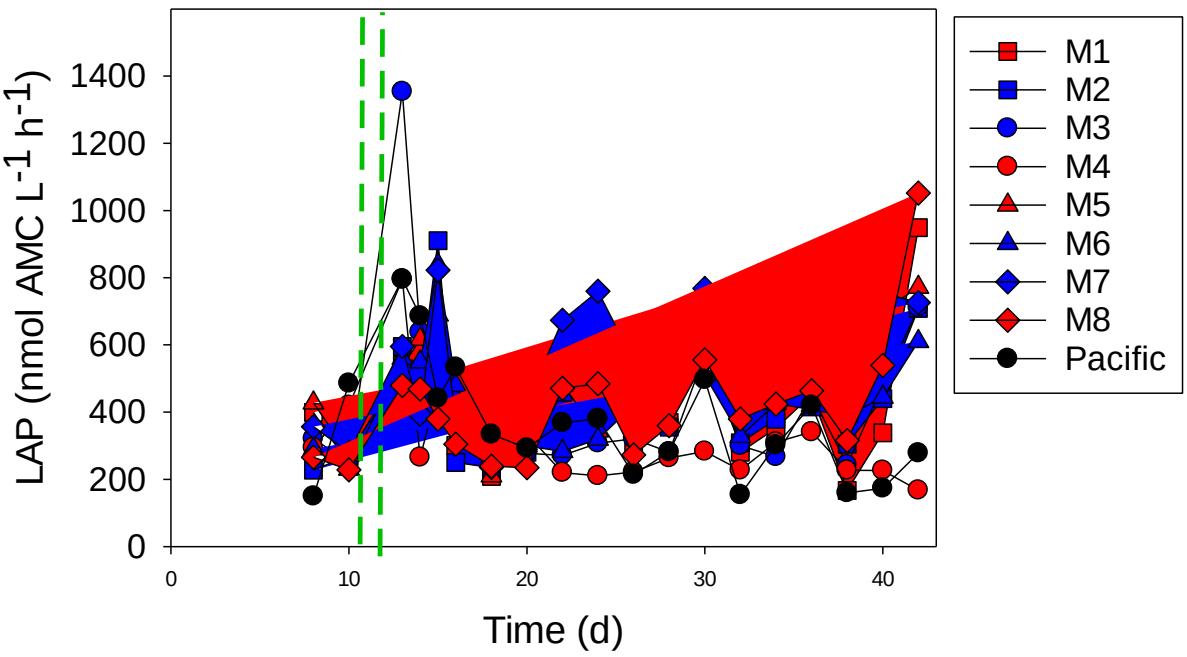

844

845 Fig 6

846

847

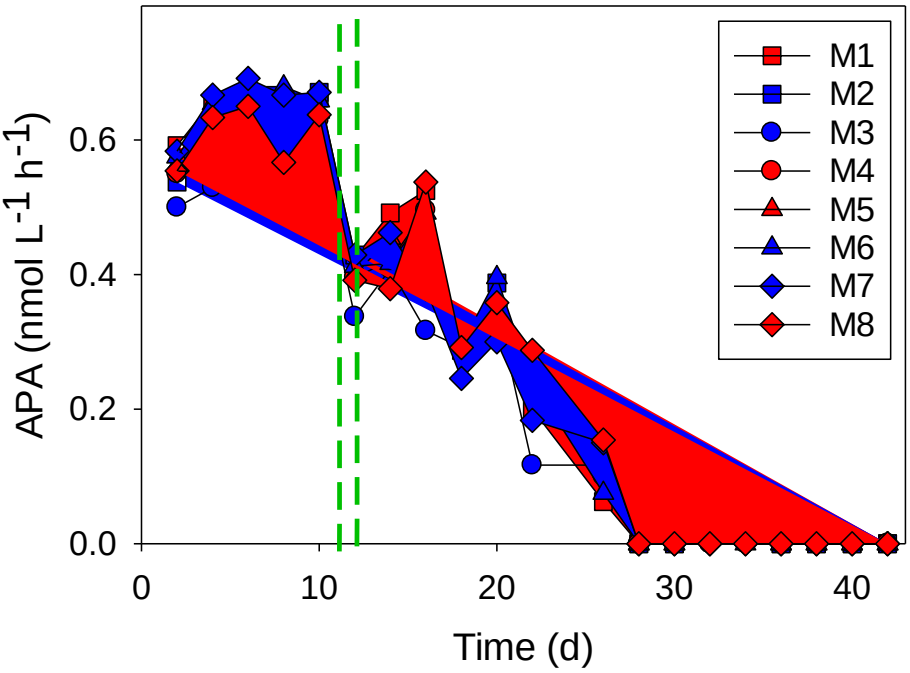

848

849 Fig 7

850

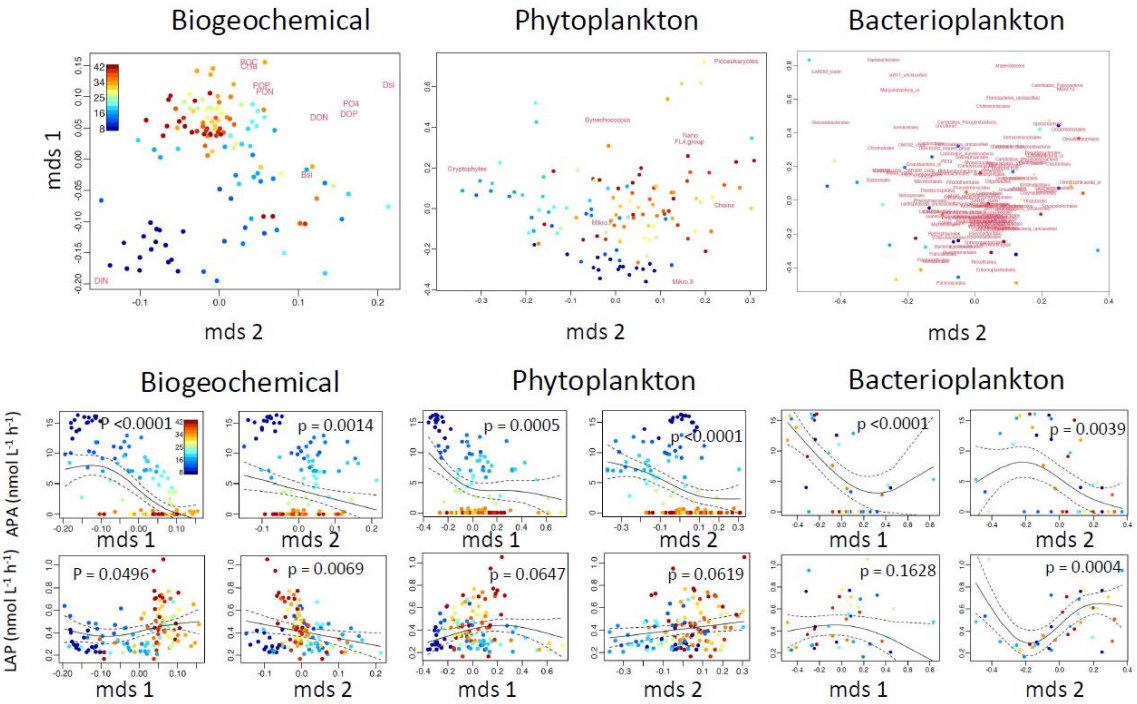

851

852 FIG 8

853

854